DALTON
FULL PAPER

Dynamic NMR investigations of fluxionality of 2-(dimethoxymethyl)-pyridine and 2,6-bis(dimethoxymethyl)pyridine in rhenium(I) and platinum(IV) complexes †

Michel L. Creber,[a] Keith G. Orrell,*[a] Anthony G. Osborne,[a] Vladimir Šik,[a] Michael B. Hursthouse[b] and K. M. Abdul Malik[c]

[a] *School of Chemistry, The University, Exeter, Devon, UK EX4 4QD. E-mail: K.G.Orrell@exeter.ac.uk*
[b] *Department of Chemistry, The University, Southampton, UK SO17 1BJ*
[c] *Department of Chemistry, University of Wales Cardiff, PO Box 912, Cardiff, UK CF1 3TB*

Received 19th July 2000, Accepted 11th September 2000
First published as an Advance Article on the web 24th October 2000

The ligands 2-(dimethoxymethyl)pyridine (L^1) and 2,6-bis(dimethoxymethyl)pyridine (L^2) formed bidentate chelate complexes with the isoelectronic transition metal moieties $Re^IX(CO)_3$ and $Pt^{IV}XMe_3$ (X = halide). The complexes $[ReX(CO)_3L^1]$ (X = Cl or Br), $[PtXMe_3L^1]$ (X = Br or I) and $[ReBr(CO)_3L^2]$ in organic solvents were shown by NMR to undergo fluxional processes which interconvert co-ordinated and pendant OMe groups. Rates and activation energies of these fluxions were measured by NMR methods (1-dimensional bandshape analysis or 2-dimensional exchange spectroscopy). Magnitudes of $\Delta G^‡$ (298.15 K) for the fluxions were in the range 59–85 kJ mol^{-1} with the order being Re^I–L^1 > Re^I–L^2 > Pt^{IV}–L^1. A carbon–carbon bond rotation mechanism is proposed for the fluxions in the L^1 complexes and concerted C–C bond rotation/metallotropic shift processes for the L^2 complexes. Crystal structures of $[ReCl(CO)_3L^1]$ and $[PtIMe_3L^1]$ revealed distorted octahedral metal centres with N–M–O 'bite' angles of 73–75° and a *trans* relationship of the axial halide and pendant OMe group.

Introduction

Ligands that contain at least two different types of bonding group with different bond strengths to metals may be described as hemi-labile ligands.[1] Their co-ordination chemistry has recently been reviewed.[2] In solution metal complexes of such ligands may undergo partial ligand displacement reactions, *i.e.* intramolecular ligand exchange processes ('fluxional shifts').

By using methods of dynamic NMR spectroscopy we have investigated the behaviour in solution of a range of metal complexes that involve terdentate ligands acting in a bidentate mode of bonding.[3–6] We have been primarily concerned with ligands that present a N_3 donor set but have now widened the investigation to encompass hemi-labile ligands such as pyridine derivatives that present an ONO donor set.[7,8]

In this paper we report on the synthesis and dynamic NMR spectroscopy of the complexes $[ReX(CO)_3L^1]$ (X = Cl or Br), $[PtXMe_3L^1]$ (X = Br or I) and $[ReBr(CO)_3L^2]$ (L^1 = 2-dimethoxymethylpyridine, L^2 = 2,6-bis(dimethoxymethyl)-pyridine). To the best of our knowledge L^1 has not been reported as a ligand and the only metal complexes reported for L^2 are $Cu(L^2)_2Cl_2$ and $Pd(L^2)_2Cl_2$ in which the L^2 molecules were considered to be co-ordinating as N-bonded monodentate ligands.[9] Somewhat related complexes of Re^I derived from a pyridine-based ligand with cyclic acetal groups in the 2,6 positions have recently been reported.[10]

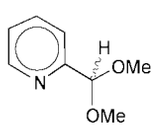

L^1

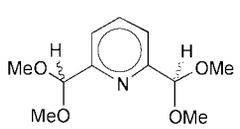

L^2

† Electronic supplementary information (ESI) available: characterisation data for rhenium(I) and platinum(IV) complexes of L^1 and L^2, mixing times and relative isomer populations used in 2-D EXSY NMR experiments. See http://www.rsc.org/suppdata/dt/b0/b005821l/

Experimental

Materials

The compounds $[ReX(CO)_5]$[11] (X = Cl or Br), $[PtXMe_3]_4$ (X = Br or I),[12] 2-dimethoxymethylpyridine[9] (L^1) and 2,6-bis(dimethoxymethyl)pyridine[9] (L^2) were prepared by adapting literature methods.

Synthesis of complexes

All preparations were carried out using standard Schlenk techniques under purified nitrogen, and with freshly distilled and degassed solvents. In a typical synthesis *ca.* 0.25 mmol of the appropriate metal precursor halide was refluxed in benzene (20 cm^3) with a small molar excess of the ligand L^1 or L^2. The solvent was removed *in vacuo*, and the solid produced dissolved in the minimum volume of CH_2Cl_2 (*ca.* 2 cm^3). The solution was transferred to a crystallising tube, and hexane (*ca.* 10 cm^3) carefully syringed on top so that there was minimal mixing of the two layers. The tube was left at −20 °C for *ca.* 1 week or until crystals of the product grew from solution. The solvents were syringed off and the crystals dried *in vacuo* for 4 h at 40 °C.

Physical methods

Elemental analyses were carried out by CHN Microanalyses, South Wigston, Leicestershire, UK. Melting temperatures were recorded on a Gallenkamp apparatus, and are uncorrected. Infrared spectra were recorded on a Nicolet Magna FT-IR instrument. ^1H NMR spectra were recorded on a Bruker DRX400 instrument operating at 400.13 MHz. All chemical shifts are quoted relative to $SiMe_4$. Variable temperature NMR spectra were obtained using the Bruker variable temperature unit B-VT2000 to control the probe temperature, calibration

 DOI: 10.1039/b005821l

Table 1 ^{1}H NMR data[a] (400.13 MHz) for L^1 in $CDCl_3$ at 303 K and the complexes *fac*-[ReX(CO)$_3$L^1] (X = Cl or Br) in $(CDCl_2)_2$ at 303 K and *fac*-[PtXMe$_3$L^2] (X = Br or I) in $CDCl_3$ at 213 K

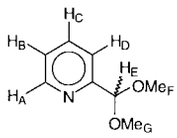

L^1

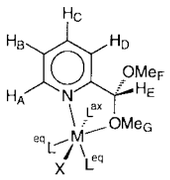

trans (major)

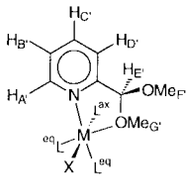

cis (minor)

Compound	$\delta_{A,A'}$ $^3J_{Pt-H}$ J_{AB}	$\delta_{B,B'}$ J_{BC}	$\delta_{C,C'}$ J_{CD}	$\delta_{D,D'}$ J_{DC}	$\delta_{E,E'}$	$\delta_{F,F'}$	$\delta_{G,G'}$	$^3J_{Pt-H}$	$\delta_{Pt-Me(eq)}$ $^2J_{Pt-H}$	$\delta_{Pt-Me(eq)}$ $^2J_{Pt-H}$	$\delta_{Pt-Me(ax)}$ $^2J_{Pt-H}$
L^1	d, 8.1 7.6(A)	t, 7.2(B) 7.6	t, 6.7(C) 7.5	d, 7.0(D) 7.5	s, 4.9(E)	s, 2.8(F)	s, 2.8(G)		—	—	—
fac-[ReCl(CO)$_3$L^1]	d, 8.85 6.7(A)	t, 8.10	t, 7.55	d, 7.65	s, 6.20(E)	s, 3.32(F)	s, 4.19(G)		—	—	—
	d, 8.81 6.7(A′)	6.7	8.0	8.1	s, 5.95(E′)	s, 3.36(F′)	s, 4.13(G′)				
	—	*b*	*b*	*b*							
fac-[ReBr(CO)$_3$L^1]	d, 8.81 6.6(A)	t, 8.08	t, 7.55	d, 7.62	s, 6.17(E)	s, 3.32(F)	s, 4.18(G)		—	—	—
	d, 8.81 6.6(A′)	6.7	7.9	8.0	s, 5.94(E′)	s, 3.38(F′)	s, 4.13(G′)				
	—	*b*	*b*	*b*							
fac-[PtBrMe$_3$L^1]	d, 8.58 7.0	t, 8.02	t, 7.59	d, 7.60	s, 6.20(E)	s, 3.24(F)	s, 3.86(G),	6.0	1.53	1.24	0.80
	15.2	7.9	7.9	8.1	s, 5.95(E′)	s, 3.27(F′)	s, 3.76(G′),	6.0	86.8	69.6	72.8
	b	*b*	*b*	*b*							
fac-[PtIMe$_3$L^1]	d, 8.60 6.9	t, 8.05	t, 7.62	d, 7.65	s, 6.21(E)	s, 3.25(F)	s, 3.91(G),	6.0	1.70	1.40	0.80
	15.8	8.1	8.0	7.9	s, 6.00(E′)	s, 3.28(F′)	s, 3.78(G′)	6.0	82.6	70.3	71.2
	b	*b*	*b*	*b*							

[a] Chemical shifts (δ), relative to TMS, δ 0; s = singlet, d = doublet, t = triplet. Scalar couplings in Hz. [b] Minor signals not resolved.

being periodically checked against a Comark digital thermometer. Sample temperatures are considered to be accurate to ±1 °C. Two-dimensional exchange (EXSY) spectra were obtained using the Bruker automation program NOESYTP. Mixing times in the EXSY experiments were chosen in the range 0.2–2.0 s according to the nature of the complex and the temperature of the measurement. Rate data were derived from bandshape analyses of the ^{1}H spectra using a version of the DNMR3 program,[13] or from 2-D EXSY spectra using volume integration data in the authors D2DNMR program.[14] Activation parameters based on experimental data were calculated using the THERMO program.[15]

X-Ray crystallography

Data were collected on an Enraf Nonius FAST TV area detector diffractometer mounted at the window of a rotating anode generator operating at 50 kV, 55 mA with a molybdenum anode as described elsewhere.[16] The structures were solved by direct methods[17] and refined by full matrix least squares[18] (Table 3). All non-hydrogen atoms were refined anisotropically and hydrogen atoms placed in ideal positions and refined using a riding model. *fac*-[PtIMe$_3$L^1] contains two chemically identical molecules in the asymmetric unit. In Fig. 5 only one of these has been shown and the average bond lengths and angles employed in the discussion.

CCDC reference number 186/2181.

See http://www.rsc.org/suppdata/dt/b0/b005821l/ for crystallographic files in .cif format.

Results and discussion

The platinum(IV) complexes *fac*-[PtXMe$_3$L^1] (X = Br or I), the rhenium(I) complexes *fac*-[ReX(CO)$_3$L^1] (X = Cl or Br) and *fac*-[ReBr(CO)$_3$L^2] were isolated in good yield as yellow or red air-stable solids. They were characterised by melting temperature, elemental analysis, and IR and ^{1}H NMR spectroscopy. In the carbonyl stretching region of the infrared spectra the rhenium complexes show three strong peaks consistent with a facial arrangement of the carbonyl groups. This indicates that all the pyridine-based ligands are acting as bidentate chelate ligands by substituting two equatorial carbonyl groups of the [ReX(CO)$_5$] compound. This finding was confirmed by subsequent ^{1}H NMR studies.

Static NMR studies of L^1 complexes

The ^{1}H chemical shifts, δ, and coupling constants, J_{ij}, for the complexes are shown in Table 1. The spectra of the rhenium(I) complexes were recorded at 303 K in $(CDCl_2)_2$, whilst those of Pt^{IV} were recorded at 213 K in $CDCl_3$ in order to minimise dissociation into "free" ligand (L^1) and the metal moiety [$(PtXMe_3)_4$].

***fac*-[ReX(CO)$_3$L^1] (X = Cl or Br).** The ^{1}H NMR spectra consist of a major set of signals and a minor set, corresponding to the two isomers of the complex arising from the pendant OMe group being either *cis* or *trans* with respect to the axial halide of the metal centre (see head of Table 1). It was assumed on steric grounds that the major set of signals corresponds to the isomer in which the bulky methoxy group is oriented away (*trans*) from the axial halide of the metal centre. Whilst there was no definitive NMR evidence to support this assumption there was support from X-ray crystal data (see later).

The spectrum of *fac*-[ReBr(CO)$_3$L^1] together with the hydrogen labelling of the two isomers is shown in Fig. 1. The major set of signals consists of singlets for Me_F and Me_G, the coordinated methoxy being more deshielded than the pendant methoxy, a singlet for H_E, and the expected pattern of signals for an *ortho*-substituted pyridyl ring. The minor set of signals consists of singlets due to $Me_{F'}$, $Me_{G'}$ and $H_{E'}$ and a doublet due to $H_{A'}$. The minor signals for the other pyridyl ring protons are not distinguishable from the major set for the two isomers. The relative populations of the major and minor forms at 303 K were 82 : 18 for the complex *fac*-[ReCl(CO)$_3$ L^1] and 84 : 16 for *fac*-[ReBr(CO)$_3$L^1]. It may be expected that the larger the halide, the less likely is the formation of the *cis* isomer on steric grounds.

***fac*-[PtXMe$_3$L^1] (X = Br or I).** The ^{1}H spectra were analogous to those of the rhenium(I) complexes above but with additional singlets, plus ^{195}Pt satellites, corresponding to the methyl groups

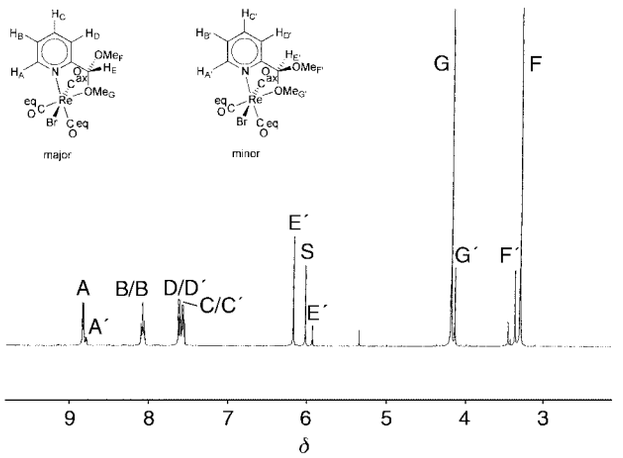

Fig. 1 400 MHz ^{1}H NMR spectrum of *fac*-[ReBr(CO)$_3$L^1] in $(CDCl_2)_2$ solvent at 303 K. S = Solvent.

of the *fac*-octahedral platinum(IV) centres. Signals for the equivalent major/minor isomers were observed, in a population ratio of 95:5 for *fac*-[PtIMe$_3$L^1] and 96:4 for *fac*-[PtBrMe$_3$L^1] at 213 K in $CDCl_3$. The assumption was again made that the major isomer contained the axial halide *trans* to the pendant methoxy group, see head of Table 1. Support for this was obtained from the crystal structure of the iodide complex, see later.

Also present in the static ^{1}H NMR spectrum were signals corresponding to the "free" ligand plus the [(PtXMe$_3$)$_4$] moiety, indicating that, despite obtaining good quality crystals, the sample dissociates in solution to its constituent parts. This suggests that the oxygen and nitrogen atoms are weaker donors to the Pt^{IV} than they are to the Re^{I}.

Oxygen inversion is invariably rapid on the ^{1}H NMR timescale, and so evidence of individual invertomers was not expected, nor was it found, in both these platinum(IV) complexes, and in the two of Re^{I}. This is in contrast to related pyridyl thioether complexes where sulfur inversion is sufficiently slow to give rise to distinguishable invertomers which undergo interconversion at rates measurable by dynamic NMR techniques.[19–22] The lowered energy barrier to inversion in ether complexes over thioether complexes (*i.e.* $O_{inv} < S_{inv}$) follows the trend $N_{inv} < P_{inv}$ for the Group 15 elements.[19]

A point of interest in the static spectra of *fac*-[PtXMe$_3$L^1] (X = Br or I) is the presence of ^{195}Pt satellites to some of the other signals apart from those due to Pt–Me. For the complex with Br, the *ortho*-pyridyl hydrogen H$_A$ shows satellites with a $^3J_{Pt\text{-}H}$ coupling of 15.2 Hz. Similarly, shoulders corresponding to partially resolved satellites were seen in the singlets for the co-ordinated methoxy groups OMe$_G$ and OMe$_{G'}$ of the major and minor isomers with $^3J_{Pt\text{-}H}$ couplings of ≈6.0 Hz. For the X = I complex similar couplings of 15.8 and ≈6 Hz respectively were noted.

NOE difference experiments were performed on *fac*-[PtIMe$_3$L^1] in $CDCl_3$ at −50 °C in order to prove the identity of the major solution isomer. However, these proved to be inconclusive. For example, irradiation of OMe$_F$ produced a small positive enhancement of the pyridyl H$_D$ signal but did not produce a similar enhancement of the axial Pt–Me signal which would have leant support to a *trans* conformation for the major isomer.

Dynamic NMR studies of L^1 complexes

***fac*-[ReX(CO)$_3$L^1] (X = Cl or Br).** Solution ^{1}H NMR variable temperature studies were performed in the range 303 to 403 K in $(CDCl_2)_2$ solution. The spectra showed that the major and minor species underwent exchange to produce, at higher temperatures, a spectrum representative of a time-averaged species

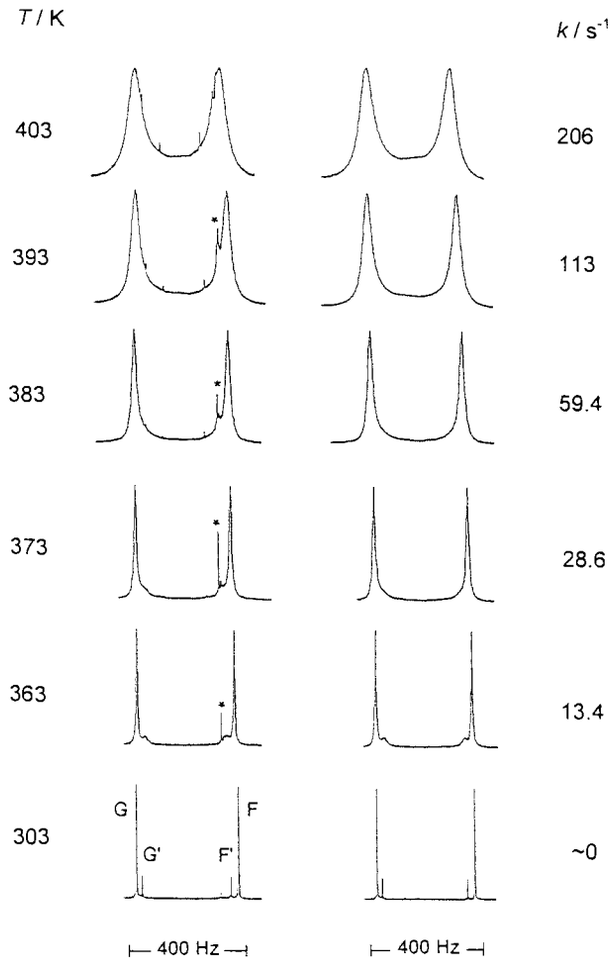

Fig. 2 Variable temperature ^{1}H NMR spectra of the methoxy signals of *fac*-[ReCl(CO)$_3$L^1] in $(CDCl_2)_2$ showing computer simulated spectra alongside; * denotes an impurity band.

due to two rapidly exchanging discrete species. Whilst the pyridyl signals were unchanged with temperature the methine signals H$_E$ and H$_{E'}$ exhibited mutual exchange, whereas in the methyl region signal Me$_F$ exchanged with Me$_{G'}$, and Me$_G$ exchanged with Me$_{F'}$, producing the spectral broadening as depicted in Fig. 2. Expansions of the experimental spectra are shown on the left, with computer simulated spectra based on 'best fit' rate constants on the right. These fittings enabled accurate activation parameters for the exchange process to be computed.

***fac*-[PtXMe$_3$L^1] (X = Br or I).** Variable temperature NMR studies were performed in the range 213 to 333 K in $CDCl_3$ solvent. In contrast to the rhenium(I) complexes above, cooling was required to arrest the exchange process that was clearly much more facile than in the former complexes. Total bandshape analysis was performed on the pairs of methoxy signals. The three signals of the platinum methyls remained sharp up to a temperature of *ca.* 283 K, beyond which all signals broadened and exchanged with each other due to a methyl scrambling process. This region was also subjected to a total bandshape analysis to measure the energy barrier for the scrambling process. Such an exchange process is a well known feature of *fac*-[PtXMe$_3$(L–L)] complexes where L–L = bidentate, chelate chalcogen ligands.[23]

On warming these platinum(IV) complexes, the proportion of "free ligand" in solution noticeably increased, pointing towards dissociation of the complex.

An important point of interest is that the ^{195}Pt satellites of the signal for the *ortho*-pyridyl hydrogen H$_A$ at 213 K were also present on this signal in the fast exchange spectrum at 333 K.

Table 2 Activation parameters for the fluxional motions in the L^1 complexes

Complex	Process	$\Delta H^{\ddagger}$/kJ mol^{-1}	$\Delta S^{\ddagger}$/J K^{-1} mol^{-1}	$\Delta G^{\ddagger}$[a]/kJ mol^{-1}
fac-[ReCl(CO)$_3$L^1]	Re–O switching	95.0 ± 1.8	35 ± 4	84.6 ± 0.2
fac-[ReBr(CO)$_3$L^1]	Re–O switching	83.6 ± 0.7	4.1 ± 1.9	82.4 ± 0.2
fac-[PtBrMe$_3$L^1]	Pt–O switching	58.7 ± 0.7	−0.7 ± 2.9	59.0 ± 0.1
	Pt–Me scrambling	82.2 ± 3.1	44.3 ± 9.8	69.0 ± 0.1
fac-[PtIMe$_3$L^1]	Pt–O switching	61.9 ± 0.8	9.3 ± 3.0	59.1 ± 0.1
	Pt–Me scrambling	85.0 ± 1.2	54.8 ± 3.9	68.7 ± 0.1

[a] Calculated at 298.15 K.

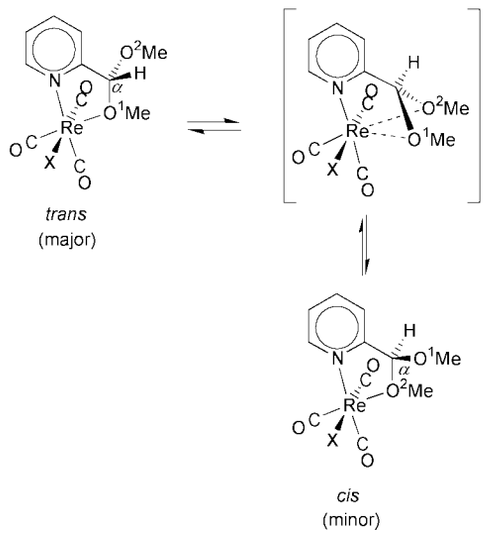

Fig. 3 Proposed mechanism for the local methoxy exchange process.

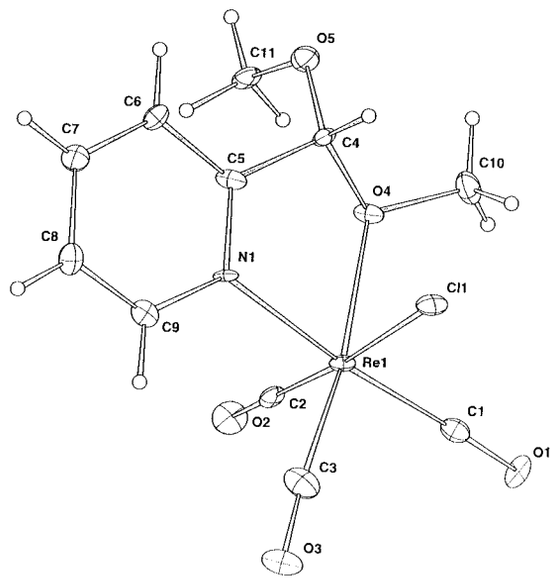

Fig. 4 Crystal structure of *fac*-[ReCl(CO)$_3$L^1] showing the atom labelling.

However, the ^{195}Pt–H couplings observed on the signals for the co-ordinated OMe groups in both isomers were either effectively zero or reduced to such an extent that they were lost within the linewidth of these signals. This will be discussed later in connection with the likely mechanism of the exchange process.

Evaluation of activation parameters

Rates for the exchange processes in all four complexes were deduced by total bandshape analysis on the signals of the methoxy or Pt–Me groups. These rates were converted into activation parameters using standard Eyring theory, Table 2. $\Delta G^{\ddagger}$ (298.15 K) values for the fluxion are in the ranges 82.4 to 84.6 kJ mol^{-1} for the rhenium(I) complexes and 59.0 to 59.1 kJ mol^{-1} for the platinum(IV) complexes. Whilst the nature of the halogen does not significantly affect the activation parameters it does affect slightly the relative populations of the major and minor solution isomers, although the trends are opposite for Re^{I} and Pt^{IV}.

The energy barriers, $\Delta G^{\ddagger}$ (298.15 K), for the Pt–Me scrambling process in the two complexes, *fac*-[PtBrMe$_3$L^1] (69.0 ± 0.1 kJ mol^{-1}), and *fac*-[PtIMe$_3$L^1] (68.7 ± 0.1 kJ mol^{-1}), also appear to be essentially independent of the halogen.

The $\Delta S^{\ddagger}$ magnitudes are close to zero (with one exception) for these isomer exchange processes, whereas the values for the methyl scrambling processes are significantly positive.

Mechanisms of the fluxional rearrangements

The spectral observations suggest a mechanism that involves an exchange of pendant and co-ordinated methoxy groups by rotation of the *ortho*-substituted moiety, as shown in Fig. 3. It is assumed to occur by a loosening of the M–O bond, rotation about the pyridyl–C_{α} bond and reco-ordination to the formerly pendant methoxy group. The M–N bond is thought to remain intact throughout this process. Support for this comes from the observations of the ^{1}H NMR spectra of *fac*-[PtXMe$_3$L^1] (X = Br or I) where ^{195}Pt satellites are observed on the signal for the *ortho*-pyridyl hydrogen. These satellites are observed at all temperatures between 213 and 333 K, irrespective of whether the exchange process is in the slow, intermediate or fast exchange regime. These satellites are a result of the $^3J_{Pt\text{-}H}$ coupling through the Pt–N bond, and indicate that the Pt–N bond remains intact during the fluxional motion. Such a mechanism is reinforced by observations from the crystallographic study of *fac*-[PtIMe$_3$L^1] (see later), where the Pt–N bond is shown to be shorter than the Pt–O bond.

The Pt–Me scrambling processes only become evident at temperatures above those associated with the onset of the methoxy exchange, and appear to be initiated by the highly fluxional nature of the 7-co-ordinate intermediates formed by the methoxy rotational exchange process. Such Pt–Me scrambling processes generally occur at rates initiated by other fluxional motions. This has been shown to be the case for chalcogen ligand complexes of $PtXMe_3$ where Pt–Me scrambling is initiated by the onset of rapid sulfur or selenium inversion or 1,3-metallotropic shifts and may occur *via* a rotation mechanism involving all three methyl groups.[23]

X-Ray crystallographic studies

X-Ray crystallographic determinations of *fac*-[ReCl(CO)$_3$L^1] and *fac*-[PtIMe$_3$L^1] were carried out in order to establish the solid-state structures of the complexes, which in turn would reinforce the assignment of the major/minor species in solution. The two labelled structures are shown in Figs. 4 and 5, with selected bond distances and bond angles listed in Tables 4 and 5 respectively. It should be noted that there are two molecules in the asymmetric unit of the platinum(IV) complex, compared to a single molecule of the rhenium(I) complex. Fig. 5 depicts one

Table 3 X-Ray crystallographic data, details of collection and structure refinement for *fac*-[ReCl(CO)$_3$L^1] and *fac*-[PtIMe$_3$L^1]

Empirical formula	$C_{11}H_{11}ClNO_5Re$	$C_{11}H_{20}INO_2Pt$
Formula weight (M)	458.86	520.27
Crystal system	Monoclinic	Triclinic
Space group	Cc (no. 9)	$P\bar{1}$ (no. 2)
a/Å	6.7128(7)	8.939(2)
b/Å	8.2692(12)	12.575(5)
c/Å	12.497(2)	14.183(4)
α/°	—	79.66(2)
β/°	104.418(11)	73.25(2)
γ/°		87.47(3)
V/Å^3	671.9(2)	1501.8(8)
Z	2	4
T/K	150(2)	150(2)
μ/mm^{-1}	9.256	11.387
Reflections collected	2721	10864
Independent reflections	1433 [R(int) = 0.0816]	3890 [R(int) = 0.0583]
Final $R1$, $wR2$ indices [$I > 2\sigma(I)$]	0.0509, 0.1243	0.0502, 0.1260
(all data)	0.0519, 0.1246	0.0649, 0.1323

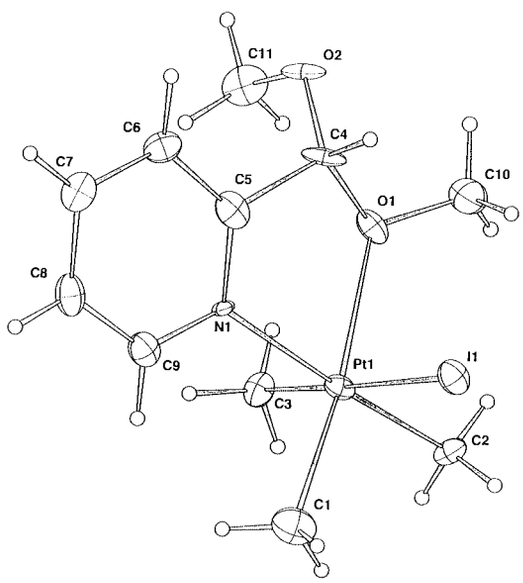

Fig. 5 Crystal structure of *fac*-[PtIMe$_3$L^1] showing one of the two molecules in the unit cell with its atom labelling.

of these two molecules, whereas Table 5 contains selected bond lengths and angles for both.

The two complexes have very similar features, most noticeably the *trans* relationship of the axial halide groups and the pendant methoxy group. This is perhaps not surprising in view of the somewhat smaller steric requirements of the axial CO or Me groups compared to those of halide. Both structures show distorted octahedral metal centres, with the 'bite angle' N(1)–Re(1)–O(4) (73.5°) being similar to that of N(1)–Pt(1)–O(1) (75.5° av.). For Re$^{\mathrm{I}}$ the lengths of the Re–N and Re–O bonds are 2.169 and 2.208 Å, respectively, whereas for Pt$^{\mathrm{IV}}$ the Pt–N and Pt–O lengths are 2.181 (av.) and 2.267 Å (av.). Thus, in both complexes, the M–N bond is significantly shorter than the M–O bond, supporting the proposed rotation mechanism for interconversion between the isomers involving breaking/remaking of the M–O bond only, with the M–N bond remaining intact at all temperatures.

The Re(1)–O(4)–C(10) angle is 117.1°, close to that expected (120°) for a trigonal planar centre. This observation is also mirrored in the *fac*-[PtIMe$_3$L^1] complex, where the angle Pt(1)–O(1)–C(10) is 119.95° (av.).The rapid oxygen inversion apparent in the solution NMR experiments may also occur in the solid state and the near trigonal planar configuration of the oxygen atoms in both complexes implies that this may be so.

Table 4 Selected bond lengths (Å) and bond angles (°) for the complex *fac*-[ReCl(CO)$_3$L^1]

Re(1)–C(3)	1.85(2)	Re(1)–C(2)	1.92(3)
Re(1)–C(1)	1.95(2)	Re(1)–N(1)	2.169(13)
Re(1)–O(4)	2.208(12)	Re(1)–Cl(1)	2.476(5)
O(1)–C(1)	1.12(2)	O(2)–C(2)	1.18(3)
O(3)–C(3)	1.21(3)	O(4)–C(4)	1.42(2)
O(4)–C(10)	1.47(2)	O(5)–C(4)	1.37(3)
O(5)–C(11)	1.45(3)	N(1)–C(5)	1.34(2)
		C(4)–C(5)	1.55(2)
C(3)–Re(1)–C(2)	85.1(9)	C(3)–Re(1)–C(1)	86.7(9)
C(2)–Re(1)–C(1)	89.2(9)	C(3)–Re(1)–N(1)	98.3(7)
C(2)–Re(1)–N(1)	93.7(7)	C(1)–Re(1)–N(1)	174.4(7)
C(3)–Re(1)–O(4)	171.4(8)	C(2)–Re(1)–O(4)	92.7(7)
C(1)–Re(1)–O(4)	101.6(7)	N(1)–Re(1)–O(4)	73.5(4)
C(3)–Re(1)–Cl(1)	99.5(7)	O(5)–C(4)–O(4)	112(2)
C(1)–Re(1)–Cl(1)	93.1(7)	N(1)–Re(1)–Cl(1)	83.6(4)
O(4)–Re(1)–Cl(1)	82.5(4)	C(4)–O(4)–C(10)	111(2)
C(4)–O(4)–Re(1)	117.9(10)	C(10)–O(4)–Re(1)	117.1(12)
C(4)–O(5)–C(11)	116(2)	O(4)–C(4)–C(5)	106.7(14)
C(5)–N(1)–Re(1)	118.3(11)	N(1)–C(5)–C(4)	118(2)
O(1)–C(1)–Re(1)	178(2)	O(5)–C(4)–C(5)	113(2)
O(3)–C(3)–Re(1)	175(2)		

Table 5 Selected bond lengths (Å) and bond angles (°) for the two molecules of the complex *fac*-[PtIMe$_3$L^1] in the asymmetric unit

Molecule 1			
Pt(1)–C(1)	2.05(2)	Pt(1)–C(3)	2.05(2)
Pt(1)–C(2)	2.06(2)	Pt(1)–N(1)	2.178(12)
C(4)–C(5)	1.55(2)	Pt(1)–O(1)	2.269(11)
O(1)–C(10)	1.40(2)	Pt(1)–I(1)	2.791(2)
O(2)–C(4)	1.37(2)	O(1)–C(4)	1.45(2)
N(1)–C(9)	1.32(2)	O(2)–C(11)	1.43(2)
		N(1)–C(5)	1.34(2)
C(10)–O(1)–C(4)	111.1(12)	C(10)–O(1)–Pt(1)	119.8(11)
C(4)–O(1)–Pt(1)	115.7(8)	C(1)–Pt(1)–N(1)	98.8(6)
C(5)–N(1)–Pt(1)	116.3(10)	C(4)–O(2)–C(11)	115.4(13)
O(2)–C(4)–O(1)	108.7(13)	O(2)–C(4)–C(5)	115(2)
C(2)–Pt(1)–O(1)	100.5(5)	N(1)–Pt(1)–O(1)	75.2(4)
O(1)–C(4)–C(5)	107.1(12)	C(3)–Pt(1)–I(1)	177.5(5)
N(1)–C(5)–C(4)	122(2)	N(1)–Pt(1)–I(1)	89.6(3)
Molecule 2			
Pt(2)–C(12)	2.05(2)	Pt(2)–C(14)	2.118(14)
Pt(2)–C(13)	2.09(2)	Pt(2)–N(2)	2.183(13)
C(15)–C(16)	1.52(2)	Pt(2)–O(3)	2.265(10)
O(3)–C(21)	1.46(2)	Pt(2)–I(2)	2.785(2)
O(4)–C(15)	1.42(2)	O(3)–C(15)	1.44(2)
N(2)–C(20)	1.37(2)	O(4)–C(22)	1.44(2)
		N(2)–C(16)	1.35(2)
C(21)–O(3)–C(15)	111.3(11)	C(21)–O(3)–Pt(2)	120.1(9)
C(15)–O(3)–Pt(2)	114.6(8)	C(12)–Pt(2)–N(2)	97.1(7)
C(16)–N(2)–Pt(2)	116.2(9)	C(15)–O(4)–C(22)	115.0(12)
O(4)–C(15)–O(3)	109.7(12)	O(4)–C(15)–C(16)	110.8(12)
C(13)–Pt(2)–O(3)	98.4(6)	N(2)–Pt(2)–O(3)	75.8(4)
O(3)–C(15)–C(16)	110.8(11)	C(14)–Pt(2)–I(2)	176.9(4)
N(2)–C(16)–C(15)	119.9(13)	N(2)–Pt(2)–I(2)	92.1(3)

NMR studies of the L^2 complex *fac*-[ReBr(CO)$_3$L^2]

This complex was prepared in the usual manner from the reaction of the ligand with rhenium pentacarbonyl bromide in benzene. A good yield of the complex was afforded. The dark red crystals melted at 191 °C with decomposition. The complex yielded results in good agreement for the elemental analysis of C, H and N. Its infrared spectrum and low temperature ^{1}H NMR spectrum confirm that the ligand acts in a bidentate chelate mode, with the ancillary CO groups in a *facial* configuration. Although the L^2 ligand contains four potential oxygen donors towards metals, chelate co-ordination will involve the pyridyl nitrogen and only one of the oxygens from either dimethoxymethyl group, but two stereoisomers are again

Table 6 ^{1}H NMR data[a] for L^2 in $CDCl_3$ at 303 K and *fac*-[ReBr(CO)$_3$L^2] in $(CDCl_2)_2$ at 253 K

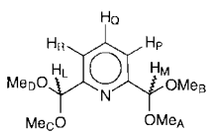

L^2

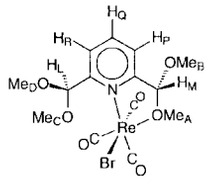

trans (major)

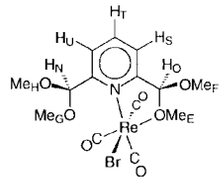

cis (minor)

Compound	$\delta_{P/S}$ J_{PQ}	$\delta_{Q/T}$ J_{QR}	$\delta_{R/U}$ J_{RQ}	$\delta_{L/N}$	$\delta_{M/O}$	$\delta Me_{A/E}$	$\delta Me_{D/H\ or\ C/G}$	$\delta Me_{B/F}$	$\delta Me_{C/G\ or\ D/H}$
L^2	d, 7.4(P) 7.5	t, 7.7(Q) 7.5	d, 7.4(R) 7.5	s, 5.3(L)	s, 5.3(M)	s, 3.3(A)	s, 3.3(D or C)	s, 3.3(B)	s,3.3(C or D)
fac-[ReBr(CO)$_3$L^2]	d, 7.61 7.7 *b*	t, 8.10 7.8 *b*	d, 8.05 7.8 *b*	s, 5.84(L) s, 5.87(N)	s, 6.20(M) s, 5.96(O)	s, 4.19(A) s, 4.13(E)	s, 3.50 major s, 3.52 minor	s, 3.29(B) s, 3.34(F)	s, 3.24 major s, 3.25 minor

[a] Chemical shifts (δ) quoted relative to TMS, δ 0; s = singlet, d = doublet, t = triplet; scalar couplings in Hz. [b] Minor shifts not resolved.

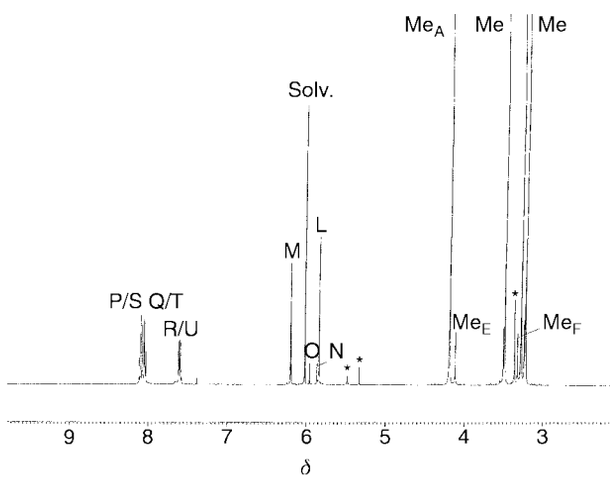

Fig. 6 400 MHz ^{1}H NMR spectrum of *fac*-[ReBr(CO)$_3$L^2] in $(CDCl_2)_2$ solvent at 253 K. Solv. denotes solvent band, * an impurity band.

possible dependent on the configuration at the C_α carbon of the chelate ring. These isomers in fact form enantiomeric pairs if involvement of the other dimethoxymethyl group is considered. NMR distinction within these isomeric pairs is not possible but exchange between them is measurable, see later.

Static studies. The ^{1}H chemical shifts, δ, and coupling constants, J_{ij}, for the complex are recorded in Table 6. The ^{1}H spectrum (Fig. 6) was recorded in $(CDCl_2)_2$ at 253 K and shows signals attributable to major and minor species in solution in the ratio 86 : 14, analogous to that obtained for *fac*-[ReBr(CO)$_3$L^1].

It was assumed, by analogy with the L^1 complexes, that the major species in solution is that in which the pendant methoxy group on the co-ordinated arm of the ligand is *trans* to the axial halide, see structures at the head of Table 6. The orientation of the pendant $CH(OMe)_2$ function is arbitrary but as the carbon atom is a prochiral centre the two methoxy groups are diastereotopic and anisochronous, irrespective of the rate of rotation about the C–C bond.

The signals for the pyridyl ring hydrogens are the expected doublet, triplet, doublet pattern for a bidentate complex of a 2,6-substituted pyridyl species. The methine region (*ca.* δ 5.5–6.5) shows four signals, two major and two minor, corresponding to the methine hydrogens in the *trans* and *cis* isomers respectively. The methoxy region shows four signals for the major (*trans*) isomer and four signals for the minor (*cis*) isomer. Two of these are noticeably shifted to high frequency, and are attributed to the co-ordinated methoxy groups in the two isomers. The other six (three major and three minor) correspond to the unco-ordinated methoxy groups in the two isomers and are assigned as far as possible.

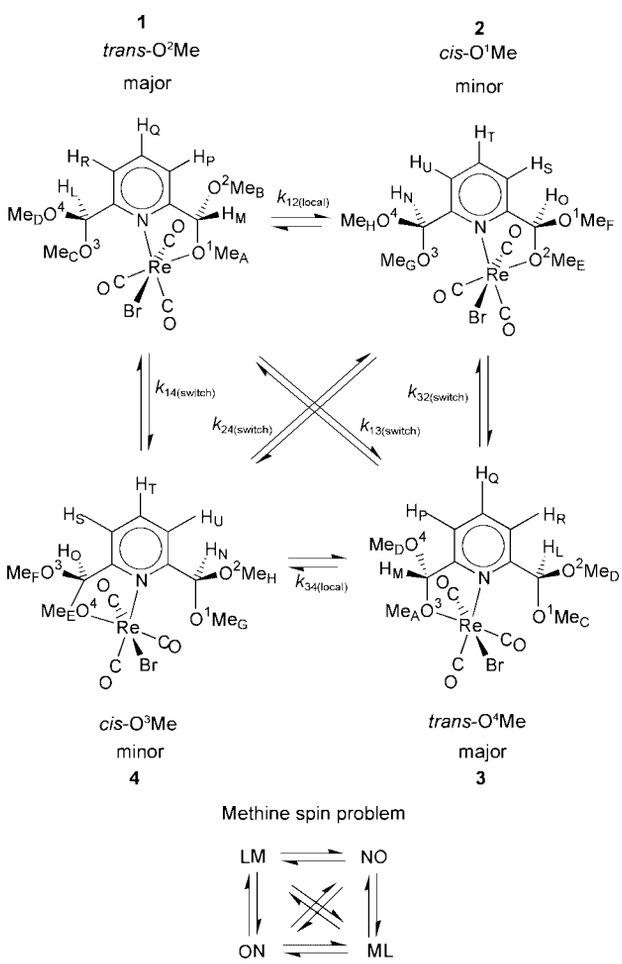

Fig. 7 Fluxional exchange pathways for the complex *fac*-[ReBr(CO)$_3$L^2] and the dynamic spin system for the methine hydrogens.

Dynamic studies. On warming the $(CDCl_2)_2$ solution of the complex to *ca.* 393 K exchange broadening of all its ^{1}H NMR signals was observed, with the notable exception of the signal for the hydrogens Q and T in the pyridyl 4 position. The signals for the pyridyl 3- and 5-hydrogens, however, did exhibit mutual exchange. In the methine region, all four signals broadened and exchanged with each other. Likewise, in the methoxy region, all eight signals exchanged with each other.

These observations can be fully explained on the basis of exchange occurring between the four isomeric structures shown in Fig. 7. These structures (labelled **1**–**4**) comprise two enantiomeric pairs, the two *trans* isomers (**1** and **3**) forming one pair and the two *cis* isomers (**2** and **4**) the other pair. There are six possible exchange pathways between these structures. The **1** ⟸⟹ **2** and **3** ⟸⟹ **4** exchanges are analogous to the *cis–trans* isomer exchanges of the L^1 complexes above. They involve exchange between co-ordinated and pendant methoxy groups arising from rotations about the C–C_a bond on the co-ordinated flank of the complex. These local rotations occur with retention of the Re–N bond. The **1** ⟸⟹ **4** and **3** ⟸⟹ **2** exchanges involve switchings of the rhenium co-ordination between the two $CH(OMe)_2$ functions with a concomitant change of configuration of the bound $CH(OMe)_2$ group leading to *trans–cis* interconversion. The **1** ⟸⟹ **3** and **2** ⟸⟹ **4** exchanges lead to switching of the rhenium co-ordination with retention of configuration, namely, *trans–trans* and *cis–cis* exchanges, respectively. There are, therefore, six independent exchange pathways of which four are NMR distinguishable. These are characterised by the rate constants, namely k_{12} (= k_{34}), k_{14} (= k_{32}), k_{13} and k_{24}, see Fig. 7. As the exchange-broadened spectra were functions of four magnitudes of rate constant it was impracticable to perform bandshape analysis to yield unique sets of 'best-fit' rate constants. Such multi-site exchange systems are, however, well suited to two-dimensional exchange spectroscopy (2-D EXSY) and so this approach was adopted.

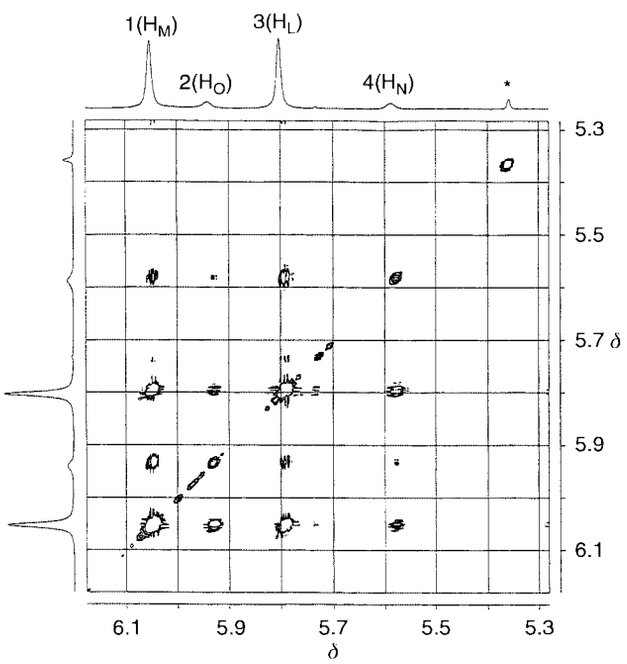

Fig. 8 ^{1}H 2-D EXSY NMR spectrum of the methine signals of *fac*-[$ReBr(CO)_3L^2$] at 283 K in $CDCl_3$–C_6D_6. Mixing time was 0.50 s. * Denotes an impurity band.

Table 7 Rate constants for the exchange pathways as shown in Fig. 9

T/°C	$k_{12/34}$/s^{-1}	k_{13}/s^{-1}	$k_{14/32}$/s^{-1}	k_{24}/s^{-1}
−20	0.031	≈0	≈0	≈0
0	0.410	0.34	0.038	≈0
5	0.69 ± 0.03	0.65 ± 0.02	0.036 ± 0.01	≈0
10	1.03	1.11	0.093	≈0
15	1.54 ± 0.06	1.87 ± 0.09	0.18 ± 0.04	≈0
20	2.04 ± 0.08	3.08 ± 0.15	0.40 ± 0.06	≈0

2-D EXSY Experiments. This technique depends on accurate volume integration of exchanging signals. The four methine signals were chosen for this purpose and a mixed solvent system ($CDCl_3$–C_6D_6) to give good separation between all signals in the range δ 5.5 to 6.1. ^{1}H 2-D EXSY spectra were recorded at seven temperatures in the range 253 to 293 K, at which magnetisation transfer was easily detected but where there was negligible exchange broadening of signals. Mixing times between the second and third 90° pulses were carefully chosen in accordance with earlier work [14] to give optimal accuracy of rate data. The 2-D EXSY spectrum measured at 283 K is shown in Fig. 8. The methine signals represent a 4-site exchange system and exchange cross peaks are observed between all signals.The relative intensities of diagonal and cross peaks form a 4 × 4 intensity matrix which was symmetrised, and normalised relative to the element I_{11}, prior to calculation. After inputting the relative populations of the *cis* and *trans* isomers as a 4 × 1 population matrix and performing the necessary matrix algebra, a kinetic matrix was calculated which contained the twelve forward and reverse rate constants as its off-diagonal elements. Forward rate constants for six temperatures are listed in Table 7. It will be noted that the rate constants k_{24} for exchange between the enantiomeric pair of minor *cis* isomers were zero within experimental accuracy. The weak cross-peaks observed between signals 2 and 4 therefore represent second-order effects [24,25] due to the mixing time not being properly optimised for this exchange pathway.

Activation parameters and mechanisms of fluxions in fac-[$ReBr(CO)_3L^2$]. Activation energy data were calculated from least-squares fittings of Eyring plots and are listed in Table 8. Owing to the rather limited temperature range within which 2-D EXSY spectra were able to be measured the entropies of activation $\Delta S^{\ddagger}$ had rather high uncertainties but were still around zero. The three fluxional processes involving exchange of co-ordinated and unco-ordinated methoxy groups, namely (i) local exchange within the bound $CH(OMe)_2$ group (based on k_{12}, k_{34} values), (ii) exchange between the two $CH(OMe)_2$ groups and involving *trans–cis* exchange (based on k_{14}, k_{32} values) and (iii) exchange between the two $CH(OMe)_2$ groups and involving *trans–trans* exchange (based on k_{13} values), all had energies of similar magnitude with process (ii) being slightly higher than the others. The activation energy of the fourth process, that involving metallotropic shifts with *cis–cis* interconversion, could not be calculated as exchange rates were negligibly slow in the temperature range studied, but the implication is that the activation energy is considerably higher than those for the other processes.

The local rotation, which is postulated to occur with retention of the Re–N bond, occurs with substantially lower energy ($\Delta G^{\ddagger}$ = 69.6 ± 0.3 kJ mol^{-1}) compared to the equivalent motion in *fac*-[$ReBr(CO)_3L^1$] where $\Delta G^{\ddagger}$ = 82.4 ± 0.2 kJ mol^{-1} (Table 2). This unexpected difference must be attributable to the pendant dimethoxymethyl substituent in the L^2 ligand having an electronic or steric effect on the pyridyl ring leading to either a

Table 8 Activation parameters for the fluxional processes in *fac*-[$ReBr(CO)_3L^2$][a]

Process	$\Delta H^{\ddagger}$/kJ mol^{-1}	$\Delta S^{\ddagger}$/J K^{-1} mol^{-1}	$\Delta G^{\ddagger}$[a]/kJ mol^{-1}
Local rotation exchange(k_{12},k_{34})	63.3 ± 3.3	−21.1 ± 12.0	69.6 ± 0.3
1,4-Metallotropic shift with *trans–cis* exchange(k_{14},k_{32})	81.6 ± 5.5	24.8 ± 46.8	74.2 ± 0.7
1,4-Metallotropic shift with *trans–trans* exchange(k_{13})	70.4 ± 1.2	5.0 ± 4.1	69.0 ± 0.1

[a] Quoted at 298.15 K.

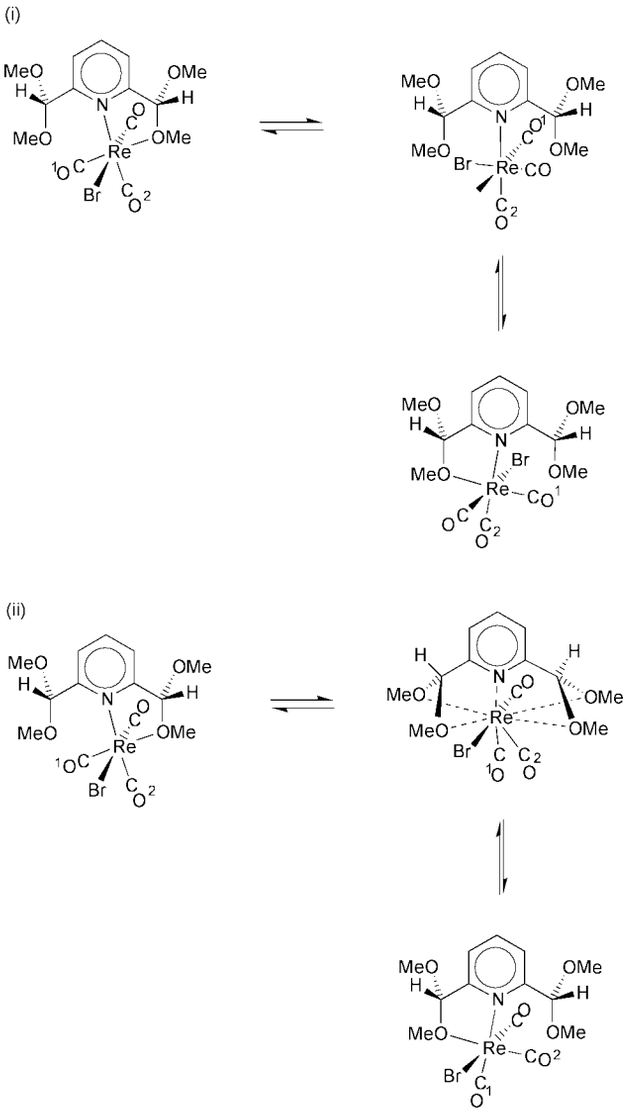

Fig. 9 Proposed metallotropic shifts of the *fac*-[ReBr(CO)$_3$L^2] complex in terms of the Re–N bond rotation mechanism (i), and the associative 'tick-tock' twist mechanism (ii).

destabilisation of the ground state energy of this L^2 complex compared to that of the L^1 complex, or to a significantly weaker Re–O bond, either effect manifesting in a much reduced activation energy for the local methoxy exchange process.

Discussion of the mechanism of the 1,4-metallotropic shifts involving switching of co-ordination between the two dimethoxymethyl groups is more speculative. Two likely mechanisms can be envisaged (Fig. 9). Mechanism (i) involves breaking of the Re–O bond as a result of the local OMe exchange followed by rotation about the Re–N bond through an angle of 180° to produce the original structure. This mechanism involves retention of the Re–N bond and a 90° transition state structure which has considerable steric crowding between the CH(OMe)$_2$ groups and the axial carbonyl and halide ligands. Mechanism (ii) involves a twist of the whole ReBr(CO)$_3$ moiety about its axial axis through an angle equal to the N–Re–O angle. It requires simultaneous loosening of both Re–N and Re–O bonds leading to a 7- or 9-co-ordinate rhenium transition state structure in which the pyridyl nitrogen atom and two, or possibly all four, methoxy oxygen atoms are involved in the bonding. This mechanism involves far less relative movement of the ligand and metal moiety, and the intermediate or transition-state structure is not sterically hindered. Such a 'tick-tock' twist mechanism has been established in *fac*-[ReX(CO)$_3$(DAP)] (DAP = 2,6-diacetylpyridine, X = halide) complexes.[8] Substantially stronger Re–N compared to Re–O bonding would obviously favour the M–N rotation mechanism (i) that does not involve any Re–N bond scission. If the Re–N and Re–O bonds are of comparable strength then the 'tick-tock' twist mechanism will be favoured. It should be noted that the energy barriers [$\Delta G^{\ddagger}$ (298.15 K)] for the switching fluxions in the present complex (69–74 kJ mol^{-1}, Table 8) are of comparable magnitude to those for the metal moiety twist fluxions in [ReBr(CO)$_3$(terpy)] (71.6 kJ mol^{-1})[26] and [ReBr(CO)$_3$(DAP)] (61.0 kJ mol^{-1})[8] and may suggest a similar mechanism.

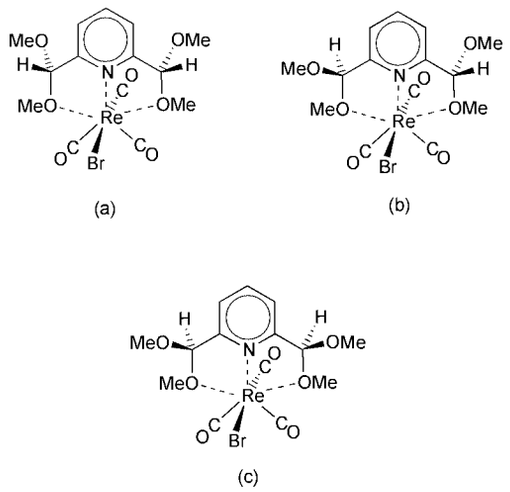

Fig. 10 Proposed transition state structures for the metallotropic shift fluxions in the *fac*-[ReBr(CO)$_3$L^2] complex.

Distinction between such 'tick-tock' twist and 'metal–N bond rotation' mechanisms can be achieved using non-racemic chiral ligands such as 2,6-bis[(4*S*)-alkyloxazolin-2-yl]pyridine as has neatly been demonstrated in recent work by Heard and co-workers.[10,27–29] This showed that both processes may occur but the 'tick-tock twist' process generally occurs more readily with an activation energy approximately 10 kJ mol^{-1} lower than for the rotation mechanism. In the present work involving the non-chiral 2-(dimethoxymethyl)pyridine and 2,6-bis(dimethoxymethyl)pyridine ligands distinction between the two pathways is possible, in theory, by the effect of the fluxion on the two equatorial environments of the rhenium moiety. The rotation mechanism (i) produces no exchange of the two carbonyl ligands (CO^1 and CO^2) attached to Re in the equatorial positions, whereas the twist mechanism (ii) will cause exchange of these two groups (Fig. 9). In the case of the DAP complexes[8] variable temperature ^{13}C NMR did reveal exchange broadening between the two equatorial carbonyls. Unfortunately, the limited quantity and solubility of the present [ReBr(CO)$_3$L^2] complex prevented any informative ^{13}C signals of the carbonyls from being obtained. However, in view of the high degree of steric congestion associated with the transition state structure of the rotation mechanism (i), the 'tick-tock' twist mechanism (ii) is the one postulated to be occurring predominantly here, but, in view of the work by Heard and co-workers,[10,27–29] the bond rotation mechanism may also be occurring albeit at a slower rate. Unfortunately the ^{1}H spectra are not sensitive to this process.

Whether the transition state structures involve co-ordination of all four methoxy oxygens or just two of them is less easy to decide. If all four were involved then a common transition state would exist for all four switching pathways (Fig. 7) and very similar activation energies might be expected for the three NMR-distinct processes. The activation energies, namely $\Delta G^{\ddagger}$ (k_{13}) = 69.0 kJ mol^{-1}, $\Delta G^{\ddagger}$ (k_{14}, k_{32}) = 74.2 kJ mol^{-1} and $\Delta G^{\ddagger}$ (k_{24}) > ≈75 kJ mol^{-1} are sufficiently different to suggest that different transition structures are indeed involved. This in turn suggests that just two methoxy oxygens are loosely bound to Re and the different energies of the transition structures (structures (a), (b) and (c), Fig. 10) arise from the different relative

orientations of the pendant OMe groups. These transition state structures relate to the *trans–trans*, *trans–cis* and *cis–cis* interconversions, respectively, implying an order of energies of (a) < (b) < (c), that may be rationalised in terms of relative steric effects.

Acknowledgements

We are most grateful to the States of Guernsey for financial support (to M. L. C.). We thank the EPSRC for use of the X-Ray Crystallographic Service when it was at the University of Wales, Cardiff, UK.

References

1 J. C. Jeffrey and T. B. Rauchfuss, *Inorg. Chem.*, 1979, **18**, 2658.
2 C. S. Slone, D. A. Weinberger and C. A. Mirkin, *Prog. Inorg. Chem.*, 1999, **48**, 233.
3 E. W. Abel, K. G. Orrell, A. G. Osborne, H. M. Pain, V. Šik, M. B. Hursthouse and K. M. A. Malik, *J. Chem. Soc.*, *Dalton Trans.*, 1994, 3441.
4 M. A. M. Garcia, A. Gelling, D. R. Noble, K. G. Orrell, A. G. Osborne and V. Šik, *Polyhedron*, 1996, **15**, 371.
5 A. Gelling, K. G. Orrell, A. G. Osborne and V. Šik, *J. Chem. Soc.*, *Dalton Trans.*, 1998, 937.
6 A. Gelling, M. D. Olsen, K. G. Orrell, A. G. Osborne and V. Šik, *Inorg. Chim. Acta*, 1997, **264**, 257.
7 K. G. Orrell, A. G. Osborne, J. O. Prince V. Šik and D. K. Vellianitis, *Eur. J. Inorg. Chem.*, 2000, 383.
8 K. G. Orrell, A. G. Osborne, V. Šik and M. Webba da Silva, *Polyhedron*, 1995, **14**, 2797.
9 A. Salameh, B. Uff, Y. Saykali and H. A. Tayim, *J. Inorg. Nucl. Chem.*, 1980, **42**, 43.
10 P. J. Heard, P. M. King, A. D. Bain, P. Hazendonk and D. A. Tocher, *J. Chem. Soc.*, *Dalton Trans.*, 1999, 4495.
11 H. D. Kaesz, R. Bau, D. Hendrickson and J. M. Smith, *J. Am. Chem. Soc.*, 1967, **89**, 2844.
12 J. C. Baldwin and W. C. Kaska, *Inorg. Chem.*, 1975, **14**, 2020.
13 D. A. Kleier and G. Binsch, DNMR3 Program 165, Quantum Chemistry Program Exchange, Indiana University, IN, 1970.
14 E. W. Abel, T. P. J. Coston, K. G. Orrell, V. Šik and D. Stephenson, *J. Magn. Reson.*, 1986, **70**, 34.
15 V. Šik, Ph.D. thesis, University of Exeter, 1979.
16 A. A. Danopoulos, G. Wilkinson and B. Hussain-Bates, *J. Chem. Soc.*, *Dalton Trans.*, 1991, 1855.
17 G. M. Sheldrick, SHELXS 86, *Acta Crystallogr.*, *Sect. A*, 1990, **46**, 467.
18 G. M. Sheldrick, SHELX 93, Program for Crystal Structure Refinement, University of Göttingen, 1993.
19 E. W. Abel, S. K. Bhargava and K. G. Orrell, *Prog. Inorg. Chem.*, 1984, **32**, 1.
20 E. W. Abel, D. Ellis and K. G. Orrell, *J. Chem. Soc.*, *Dalton Trans.*, 1992, 2243.
21 E. W. Abel, P. J. Heard, K. G. Orrell, M. B. Hursthouse and M. A. Mazid, *J. Chem. Soc.*, *Dalton Trans.*, 1993, 3795.
22 E. W. Abel, E. S. Blackwall, M. L. Creber, P. J. Heard and K. G. Orrell, *J. Organomet. Chem.*, 1995, **490**, 83.
23 K. G. Orrell, *Coord. Chem. Rev.*, 1989, **96**, 1.
24 R. Willem, *Prog. Nucl. Magn. Reson. Spectrosc.*, 1987, **20**, 1.
25 K. G. Orrell, *Prog. Nucl. Magn. Reson. Spectrosc.*, 1990, **22**, 141.
26 E. W. Abel, V. S. Dimitrov, N. J. Long, K. G. Orrell, A. G. Osborne, H. M. Pain, V. Šik, M. B. Hursthouse and M. A. Mazid, *J. Chem. Soc.*, *Dalton Trans.*, 1993, 597.
27 P. J. Heard and C. Jones, *J. Chem. Soc.*, *Dalton Trans.*, 1997, 1083.
28 P. J. Heard and D. A. Tocher, *J. Chem. Soc.*, *Dalton Trans.*, 1998, 2169.
29 P. J. Heard, A. D. Bain and P. Hazendonk, *Can. J. Chem.*, 1999, **77**, 1707.